Lanthanide Coordination Networks Based on Diamantane-4,9-Diphosphonic Acid

Tim Müller, Peter Ferber, Philipp M. Roos, Nabil Assahub, Christoph Janiak

Suggested Citation:
Müller, T., Ferber, P., Roos, P. M., Assahub, N., & Janiak, C. (2025). Lanthanide Coordination Networks Based on Diamantane-4,9-Diphosphonic Acid. Zeitschrift Für Anorganische Und Allgemeine Chemie, 652 (1), Article e202500158. https://doi.org/10.1002/zaac.202500158

Journal of Inorganic and General Chemistry
ZAAC
Zeitschrift für anorganische und allgemeine Chemie
www.zaac.wiley-vch.de
RESEARCH ARTICLE
Check for updates
DOI: 10.1002/zaac.202500158

Lanthanide Coordination Networks Based on Diamantane-4,9-Diphosphonic Acid

Tim Müller, Peter Ferber, Philipp M. Roos, Nabil Assahub, and Christoph Janiak*

Dedicated to Prof. Dr. Mathias Wickleder on the occasion of his 60th Birthday

Four new Ln-based (Ln = Eu, Gd, Er) coordination networks, $\{[EuL_{1.5}(H_2O)_4]\cdot H_2O\}_n$ and $\{[LnL_{1.5}(H_2O)]\cdot H_2O\}_n$ (Ln = Eu, Gd, Er), were synthesized using the precursor diamantane-4,9-bis(dichlorophosphoryl) ($Diam(POCl_2)_2$) to form in situ the linker diamantane-4,9-bis(hydrogenphosphonate) ($L = Diam(PO_3H)_2^{2-}$) with singly deprotonated phosphonate groups. These coordination networks represent the first reported examples of diamantane-phosphonate networks. The combination of Ln^{3+} ions and $Diam(PO_3H)_2^{2-}$ resulted in the formation of doubly -PO_3H^- bridged Ln chains. These chains are interconnected by the diamantane moiety of the diamantane-4,9-bis(hydrogenphosphonate) linker, forming 2D (Eu) or 3D (Eu, Gd, Er) networks. In the 3D networks, Eu^{3+}, Gd^{3+}, and Er^{3+} exhibit an uncommon coordination number of 6, from five phosphonate groups and one aqua ligand. This may be due to the constraints of the 3D network but at the same time shows the adaptability of Ln^{3+} ions to coordination constraints crucial for the formation of the 3D phosphonate frameworks.

1. Introduction

Organophosphonate ligands R-PO_3^{2-} or R-PO_3H^- are highly valued in coordination chemistry for their versatility and robust binding capabilities, leading to a steady growth in their research. Phosphonate groups can bind to metal ions through up to three oxygen atoms.[1,2] The strong M—O—P bonds enhance the thermal and chemical stability of the resulting structures.[3,4] Their structural characteristics enable the formation of chemically and thermally stable coordination networks. Yet, the synthesis of porous metal-phosphonate framework structures remains challenging due to the flexibility in the metal–oxygen binding.[5,6] Both, the number of phosphonic acid groups in the linker[7] and the selected metal ion[8] are key factors in the synthesis of phosphonate-based coordination networks, together with the pH value of the synthesis medium which governs the (de)protonation state of the phosphonic acid ($pK_1 = 2–4$, $pK_2 = 4–9$).[9] One route to predictable structures could be the use of bidentate phosphonate monoesters, as they have a similar binding mode to carboxylate linkers, leaving an alkoxy group that can be modified further.[10]

Diamantane ($C_{14}H_{20}$) consists of two fused adamantane cages and can be a linear linker in metal coordination networks with donor groups at the axial bridge-head 4,9-positions (**Figure 1**). The use of diamantane-containing linkers is very limited so far, with a series of molybdenum oxide diamantane-4,9-bis(triazol-4-yl) coordination polymers[11] and a diamantane-4,9-dicarboxylate based UiO-66 analog (HHUD-3).[12] The rigid and hydrophobic structure of diamondoid cage molecules can improve the stability of materials.[13,14]

Compared to other phosphonate ligands,[15] bulky diamantane-based phosphonates offer unique structural features that could influence lanthanide coordination and could possibly introduce porosity, while the addition of phosphonate groups further broadens their chemical versatility.[12,16] Diamantanes are highly functionalizable, making them attractive for coordination chemistry application,[17,18] in catalysis, sensing, drugs, and advanced materials science.[19,20] When combined with lanthanides, some phosphonate linkers may also exhibit interesting luminescent or magnetic properties.

Lanthanide coordination networks owe a remarkable structural diversity due to the high coordination number and flexible coordination environment of the lanthanide ion.[21–23] Coordination geometry flexibility and high coordination numbers make lanthanide-based networks a promising class of materials with properties such as luminescence,[24,25] thermal stability,[26] magnetism,[27,28] and catalytic behavior.[29–31]

Lanthanide-containing materials are well known for their narrow emission bands and high color purity in both the visible (VIS) and near-infrared (NIR) regions. Among them, Eu^{3+} and Tb^{3+} are the most used lanthanide ions in luminescence applications.[32] For example, the Müller-Buschbaum group fine-tuned the luminescence color of $[Gd_2Cl_6(bipy)_3]\cdot 2bipy$ from green to red by varying the amounts of Eu^{3+} or Tb^{3+}.[33] Additionally, they synthesized the porous MOF $[Ce(Im)_3ImH]\cdot ImH$ (ImH = 1*H*imidazole), which exhibits blue luminescence and serves as a highly responsive detector for H_2O, O_2, CH_2Cl_2 and MeCN.[34]

T. Müller, P. Ferber, P. M. Roos, N. Assahub, C. Janiak
Institut für Anorganische Chemie und Strukturchemie, Heinrich-Heine-Universität Düsseldorf, 40204 Düsseldorf, Germany
E-mail: janiak@uni-duesseldorf.de

Supporting information for this article is available on the WWW under https://doi.org/10.1002/zaac.202500158

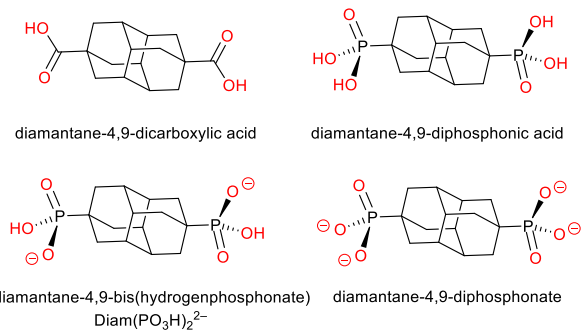

Figure 1. Structures of diamantane-4,9-dicarboxylic acid and -diphosphonic acid with the mono- and bis-deprotonated phosphonates.

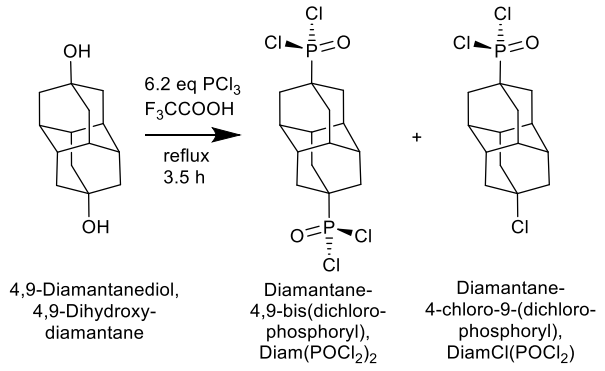

Scheme 1. Synthesis of $Diam(POCl_2)_2$ and the $DiamCl(POCl_2)$ byproduct.

Lanthanide coordination-networks have also been explored for their proton conductivity. Bazaga-García et al. reported a series of $Ln[H(O_3PCH_2)_2–NH–(CH_2)_2–SO_3]·2H_2O$ networks (Ln = La, Pr, Nd, Sm, Eu, Gd, and Tb) which have been investigated as proton-conductive materials for membrane electrode assemblies.[35] Layered Ln-oxalatophosphonates $[Ln(H_2L)(C_2O_4)]·H_2O$ [Ln = La, Ce, Pr, H_2L = $H(O_3PCh_2)_2$-NH-$(CH_2)_2$-SO_3) and $[Ln_2(H_3L)(C_2O_4)_3(H_2O)_4]·2H_2O$ [Ln = Eu and Dy, H_3L = $H(O_3PCh_2)_2$-NH-$(CH_2)_2$-SO_3H)] exhibit both characteristic luminescence and intriguing magnetic properties, such as temperature-dependent magnet behavior and antiferromagnetic interaction between Dy^{III} ions at low temperatures.

This study introduces four novel coordination networks synthesized using diamantane-4,9-bis(hydrogenphosphonate) as the linker with the lanthanides Eu^{3+}, Gd^{3+}, and Er^{3+}.

The structural similarity of the diphosphonates to dicarboxylates allows for reticular chemistry,[36–38] while the stronger M—O—P bonds may enhance thermal and chemical stability.[39,40]

2. Results and Discussion

The reaction of 4,9-dihydroxydiamantane with PCl_3 in trifluoracetic acid as described by Fokin et al.[41] afforded in our hands a mixture of the desired product diamantane-4,9-bis (dichlorophosphoryl) ($Diam(POCl_2)_2$) and of diamantane-4-chloro-9-(dichlorophosphoryl), $DiamCl(POCl_2)$ as a byproduct (**Scheme 1**). $DiamCl(POCl_2)$ probably forms with hydrochloric acid from the hydrolysis of PCl_3 with traces of water. Attempts to separate the two compounds via column chromatography were unsuccessful.

To try to separate the mixture of $Diam(POCl_2)_2$ and $DiamCl(POCl_2)$ through formation of a magnesium phosphonate network with only the hydrolysis product of $Diam(POCl_2)_2$, we reacted the mixture with methanol, $Mg(NO_3)_2·6H_2O$, water, and acetic acid in the presence of catalytic amounts of hydrochloric acid (**Scheme 2**). However, the reaction afforded no magnesium compound, but instead the product mixture contained crystals of diamantane-4,9-bis(methyl hydrogenphosphonate) ($Diam(PO_3HMe)_2$, **Figure 2**), which is the dimethyl ester of

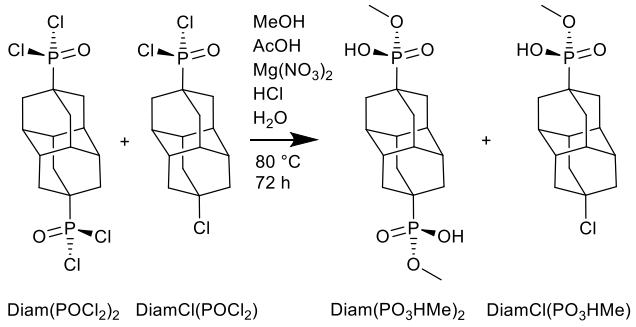

Scheme 2. Synthesis of diamantane-4,9-bis(methyl hydrogenphosphonate), ($Diam(PO_3HMe)_2$), and diamantane-4-chloro-9-(methyl hydrogenphosphonate) ($DiamCl(PO_3HMe)$).

diamantane-4,9-diphosphonic acid ($Diam(PO_3H_2)_2$), and of diamantane-4-chloro-9-(methyl hydrogenphosphonate) ($DiamCl(PO_3HMe)$, **Figure 3**) as a monohydrate. The latter is the monomethyl ester of diamantane-4-chloro-9-phosphonic acid. Both esters derive from the hydrolysis of the respective dichlorophosphoryl compounds $Diam(POCl_2)_2$ and $DiamCl(POCl_2)$ (Scheme 2).

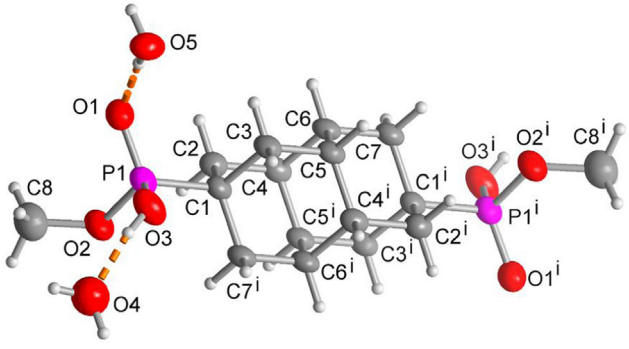

Figure 2. Molecular structure of diamantane-4,9-bis(methyl hydrogenphosphonate) ($Diam(PO_3HMe)_2$) trihydrate with two hydrogen-bonded crystal water molecules (orange dashed lines). A detailed description of the structure can be found in the Section S5, Supporting Information.

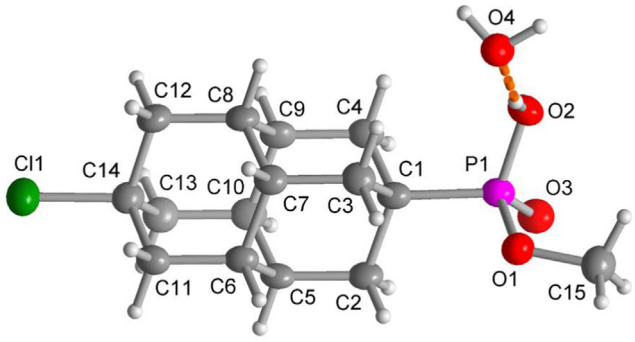

Figure 3. Molecular structure of diamantane-4-chloro-9(methyl hydrogenphosphonate) (DiamCl(PO_3HMe)) monohydrate with the hydrogen-bonded crystal water molecule (orange dashed line). A detailed description of the structure can be found in the Section S6, Supporting Information.

Commercial Diam$(POCl_2)_2$, supplied by TransMIT, served as a precursor for the in situ generation of diamantane-4,9-bis (hydrogenphosphonate) (Diam$(PO_3H)_2^{2-}$) by hydrolyzation of the P—Cl bonds under hydrothermal conditions. The slowly formed phosphonate then acted as a linker in the synthesis of four novel lanthanide-based coordination networks as well-crystallized reaction products (Figure S1, Supporting Information, **Scheme 3**). The synthesis was only successful when using p-ethylphosphonic acid (EtPA) and 4,4′-bipyridine (4,4′-BPY) or 1,4-diazabicyclo [2.2.2]octane (DABCO). EtPA served both as a well-soluble monophosphonic acid to lower the pH and as a modulator. Modulators like EtPA can influence crystallization kinetics by controlling the deprotonation of linker molecules and regulating coordination to the metal centers, in order to improve crystallinity and for morphology control. This approach is well established in the synthesis of carboxylate MOFs, where monocarboxylic acids are routinely used as modulators to control crystal growth and improve crystallinity.[42,43] 4,4′-Bipyridine and DABCO can act as a weak ligand that temporarily coordinates to the metal centers, thereby acting as a template. As a base, it can modulate the pH value and deprotonate the phosphonic acid with formation

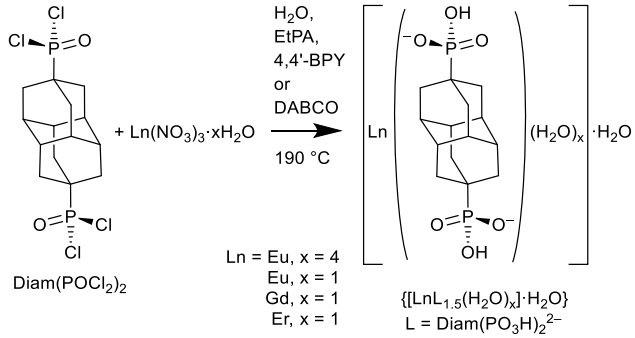

Scheme 3. In situ formation of lanthanide networks with diamantane-4,9-bis(hydrogenphosphonate), Diam$(PO_3H)_2^{2-}$ from the hydrolysis of Diam$(POCl_2)_2$. Ln = Eu, Gd, Er, EtPA = p-ethylphosphonic acid. 4,4′-BPY = 4,4′-bipyridine, DABCO = 1,4-diazabicyclo [2.2.2]octane.

of bipyridinium cations. Eventually, the EtPA modulator and 4,4′-BPY or DABCO will be displaced by the phosphonate linker, enabling the formation of the desired coordination network.[44]

The four networks were orthorhombic {[$EuL_{1.5}(H_2O)_4$]·H_2O}$_n$ (**1-o**), monoclinic {[$EuL_{1.5}(H_2O)$]·H_2O}$_n$ (**1-m**), {[$GdL_{1.5}(H_2O)$]·H_2O}$_n$ (**2**) and {[$ErL_{1.5}(H_2O)$]·H_2O}$_n$ (**3**) with L = Diam$(PO_3H)_2^{2-}$ and with the latter three networks being isostructural.

The tetraaqua europium compound {[$EuL_{1.5}(H_2O)_4$]·H_2O}$_n$ (**1-o**) crystallizes in the orthorhombic crystal system with the space group Pbca. The asymmetric unit contains one Eu atom, a fully and a half-occupied diamantane-4,9-bis(hydrogenphosphonate) linker, four aqua ligands, and a crystal water molecule (**Figure 4**). Each phosphonate group in the linker is only singly deprotonated, forming a hydrogenphosphonate (-PO_3H^-) group.

The unique Eu atom is eight-coordinated by four O atoms from four different hydrogenphosphonate (-PO_3H^-) groups and four aqua ligands (Figure 4b,c). The coordination environment around Eu adopts a distorted dodecahedral or square-antiprismatic geometry. The shape of the coordination polyhedron in {[$EuL_{1.5}(H_2O)_4$]·H_2O}$_n$ (**1-o**) is very close to square antiprism (SAPR-8) with a CShM value of 0.770 (the values of the CShM, which is the minimal mean square deviation of the vertex

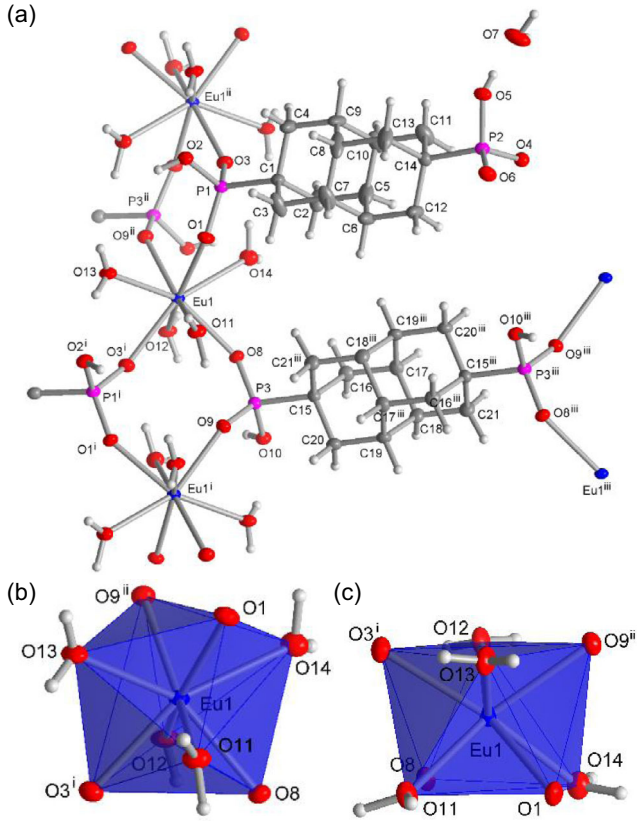

Figure 4. The extended asymmetric unit a) in {[$EuL_{1.5}(H_2O)_4$]·H_2O}$_n$ (**1-o**), and the coordination sphere around europium emphasizing the coordination as dodecahedral b) or as square-antiprismatic c) (50% thermal ellipsoids), symmetry codes: (i) $x + 1/2$, y, $-z + 1/2$; (ii) $x - 1/2$, y, $-z + 1/2$; (iii) $-x + 2$, $-y + 1$, $-z + 1$. A selection of bond distances and angles in **1-o** can be found in Table S7b, Supporting Information.

coordinates from the ideal polyhedron, were computed by the SHAPE 2.1 program,[45] and the shorthand codes of the polyhedra in the brackets follow the ones used in the program). In comparison, the triangular dodecahedron (TDD-8) is the second most corresponding among typical symmetric idealized polyhedra with a CShM value of 1.83 compared to the much more different cube (CU-8) at 6.93. It is interesting to note that while the observed shape of the $\{EuO_8\}$ is not very far from the triangular dodecahedron, it is not lying on the minimal distortion path from the square antiprism to the latter (the deviation from the path is 31.9 and generalized coordinate of 51.8 in the range of 0–100%, as calculated by SHAPE 2.1). On the other hand, the observed geometry could be viewed as lying on the minimal distortion path from the square antiprism to a cube (the deviation from the path is 4.8, while the generalized coordinate is 26.0). Thus, the actual configuration could be represented as a modest rotation of the bottom part of the prism around the original C_4 axis towards the cubic shape.

The phosphonate linker with P1 and P2 is only a bridging group at P1, coordinating two Eu atoms. The phosphonate group at P2 is not coordinated to a metal atom and is solely involved in hydrogen bonding (Figure 4a). In the linker containing P3, which sits on a special position, each phosphonate group bridges between two Eu atoms, resulting in the linker as a whole connecting four Eu atoms. Out of the four $-PO_3H^-$ groups around Eu, two with P1 and two with P3, each bridge to a neighboring Eu atom, resulting in each Eu atom being in total connected to 6 other Eu atoms (**Figure 5**).

The direct phosphonate P1 and P3 bridging action between the Eu atoms leads to a slightly corrugated doubly bridged Eu chain parallel to the crystallographic *a*-direction. Each Eu chain is "left-and-right" connected through the P3-P3′ linker to two adjacent strands (Figure 5), forming a layered 2D 6-c uninodal network with the point symbol $3^6.4^2.5^6.6$ as analyzed by ToposPro (details in Supporting Information).[46]

The hydrogen bonding scheme in **1-o** is illustrated in Figure S16, Supporting Information. The H-atoms of the hydrogenphosphonate groups ($-PO_3H^-$) are all involved in hydrogen bonding, either to other phosphonate groups or to the crystal water molecule.

The monoaqua lanthanide compounds $\{[LnL_{1.5}(H_2O)]\cdot H_2O\}_n$ (Ln = Eu (**1-m**), Gd (**2**), Er (**3**)) crystallize isostructurally in the monoclinic crystal system with the space group $P2_1/n$. Their asymmetric unit consists of one Ln^{3+} atom, a fully and half-occupied diamantane-4,9-bis(hydrogenphosphonate) linker, one aqua ligand, and a crystal water molecule. The crystal water molecule is split over two nearby positions with 0.75 and 0.25 occupancy in **1-m**, two partially occupied crystal water molecules in **2** and and two half-occupied crystal water molecules in **3**. As before, each phosphonate group is only singly deprotonated, presenting a hydrogenphosphonate (PO_3H^-) group.

In the structure of **1-m** and of **2**, the Eu^{3+} and Gd^{3+} atom are six- to seven-coordinated by five to six O atoms from five different hydrogenphosphonate ($-PO_3H^-$) groups and the aqua ligand. The sixfold coordination around Eu^{3+} and Gd^{3+} is a distorted octahedron (**Figure 6**a,b). A coordination from a long Eu1—O4^i bond of

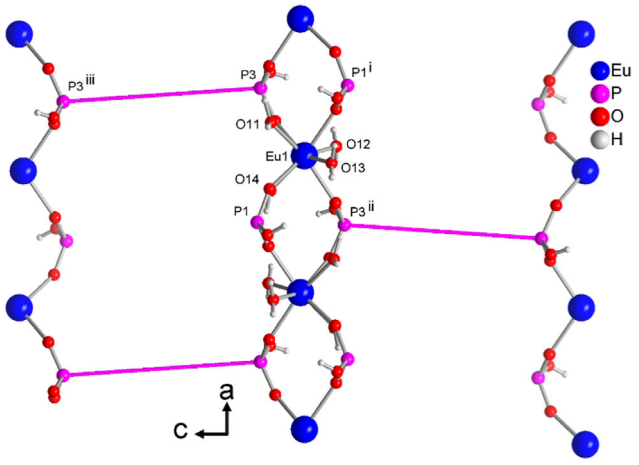

Figure 5. Schematic connectivity around Eu in **1-o** showing the connectivity to 6 neighboring Eu atoms from which two are connected directly through the P1 and P3 phosphonate groups and four across the P3-P3′ diamantane linker. The diamantane unit is replaced by a direct P—P connector in magenta for clarity (the crystal water molecules are not shown). Also, for clarity, the diamantane moiety in the P1-P2 linker, which is only metal-coordinating at P1, has been removed together with the non-coordinating P2 group (cf. Figure S15, Supporting Information). Symmetry codes: (i) $x+1/2$, y, $-z+1/2$; (ii) x $-$ 1/2, y, $-z+1/2$; (iii) $-x+2$, $-y+1$, $-z+1$.

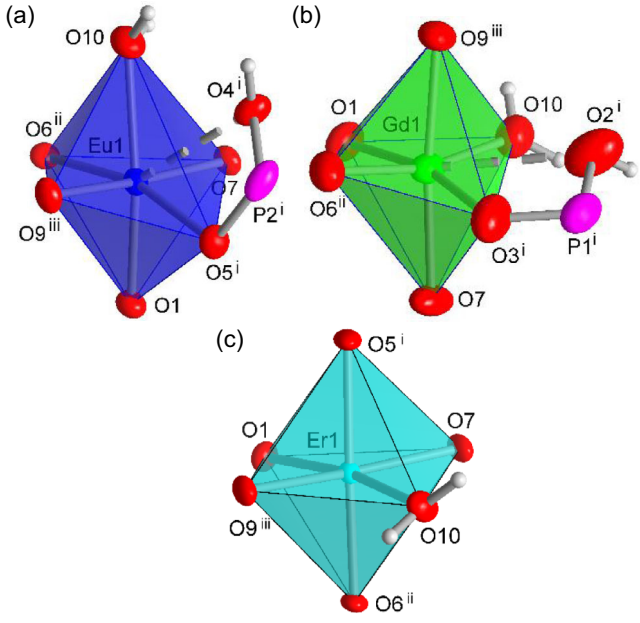

Figure 6. The coordination sphere around a) Eu^{3+} in **1-m**, b) Gd^{3+} in **2**, and c) Er^{3+} in **3** in the isostructural networks $\{[LnL_{1.5}(H_2O)]\cdot H_2O\}_n$ (50% thermal ellipsoids). Symmetry codes in **1-m**: (i) $-x+1/2$, $y+1/2$, $-z+1/2$; (ii) $x+1$, y, z; (iii) $-x+3/2$, $y+1/2$, $-z+1/2$; in **2**: (i) $-x+1/2$, $y-1/2$, $-z+3/2$; (ii) $x-1$, y, z; (iii) $-x+1/2$, $y+1/2$, $-z+3/2$; in **3**: (i) $-x+1/2$, $y+1/2$, $-z+3/2$; (ii) $x+1$, y, z; (iii) $-x+3/2$, $y-1/2$, $-z+3/2$. A selection of bond distances and angles in **1-m**, **2**, and **3** can be found in Table S9b, S11b, S13b, Supporting Information, respectively.

2.823 Å may be taken into account from a then chelating O—P—OH group (Figure 6a). The other Eu1—O bond lengths lie between 2.090 and 2.399 Å (Table S9b, Supporting Information).

The possibly sevenfold coordination of Gd^{3+} derives from a long Gd1—O2^{i} bond of 2.900 Å from a chelating O—P—OH group (Figure 6b). The other Gd1—O bond lengths lie between 2.228 and 2.401 Å (Table S11b, Supporting Information). The sevenfold coordination of Eu^{3+} and Gd^{3+} would be capped octahedrons (Figure 6a,b).

In the Er structure of **3**, the Er^{3+} atom is clearly only six-coordinated by five O atoms from five different hydrogenphosphonate (PO_3H^-) groups and an aqua ligand (Figure 6c). The Er1—O bond lengths lie between 2.178 and 2.336 Å (Table S13b, Supporting Information). The next nearest Er-O distance is over 3.7 Å. The coordination around Er is a distorted octahedron. The tendency towards sevenfold coordination of Eu^{3+} and Gd^{3+} versus the clearly sixfold coordination of Er^{3+} in the isostructural networks is evidence of the larger ionic radii of Eu^{3+} (0.947 Å) and Gd^{3+} (0.935 Å) versus Er^{3+} (0.89 Å). At the same time, it can be noted that in the structure of **1-o** Eu^{3+} was eightfold coordinated.

The lanthanide contraction leads to a systematic decrease in ionic radii from La^{3+} to Lu^{3+}, decreasing also the coordination number (CN) and influencing the ligand preferences.[47–49] The coordination number of lanthanides ranges from 6 to 12, depending on ligand size, charge, and steric effects.[50,51] Lanthanides with larger ionic radii, such as La^{3+}, Ce^{3+}, and Pr^{3+}, tend to adopt nine-coordination, whereas smaller lanthanides like Eu^{3+} and Dy^{3+} show nine- and eight-coordination.[52,53] Gadolinium(III) and erbium(III) also display CN = 8 or 9 in many complexes, though CN = 6 is observed in structures with sterically demanding ligands or strong chelating effects.[54–56]

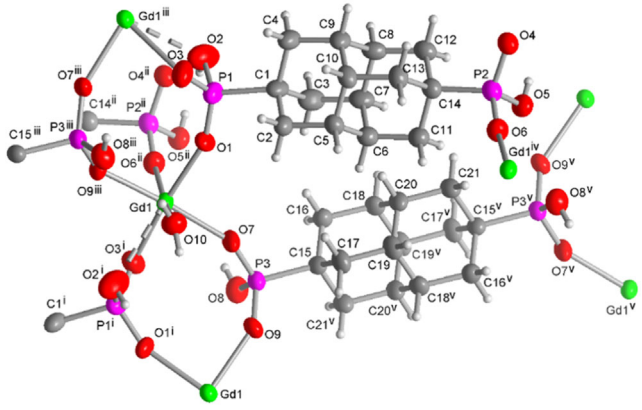

Figure 7. The extended asymmetric unit in $\{[GdL_{1.5}(H_2O)]\cdot H_2O\}_n$, not showing the minor contribution of the disordered atoms of the phosphonate group at P1. The linker containing P1 and P2 acts as a bridging group only at P1, coordinating to two Gd atoms. At P2, it is terminally coordinated to only one Gd atom. The linker with P3, which occupies a special position, connects four Gd atoms (50% thermal ellipsoids). Symmetry codes: (i) $-x+1/2$, y − 1/2, $-z+3/2$; (ii) x − 1, y, z; (iii) $-x+1/2$, $y+1/2$, $-z+3/2$; (iv) $x+1$, y, z; (v) $-x+1$, −y, $-z+1$. See Figure S17 and S24, Supporting Information for the structure images of **1-m** and **3**, respectively.

In the Ln-phosphonate structures described here, only in **1-o** does Eu^{3+} display the common CN of 8 with four phosphonate groups and four water molecules, while in **1-m**, **2**, and **3**, Eu^{3+}, Gd^{3+}, and Er^{3+} each exhibit an uncommon CN of 6, comprising five phosphonate groups and one water molecule. This may be due to the constraints of the 3D network architecture (see below) on coordination behavior.[57] Conversely, the adaptability of Ln^{3+} ions to coordination constraints is crucial for the structural diversity of their complexes and for the formation of the 3D phosphonate frameworks.[32]

We will visualize the following general network structure description with the Gd compound **2**. In the three isostructural compounds $\{[LnL_{1.5}(H_2O)]\cdot H_2O\}_n$ (Ln = Eu (**1-m**), Gd (**2**), Er (**3**)), the fully occupied linker bridges only between three Ln atoms as with one of its ends it functions as a monodentate group and is terminally coordinated to only one Ln atom (**Figure 7**).

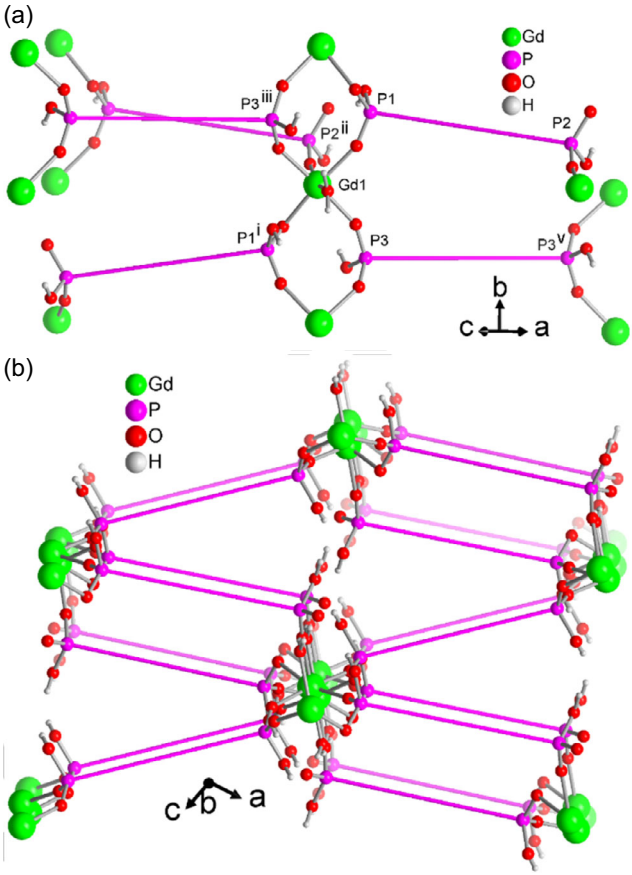

Figure 8. Schematic connectivity around Gd in **2** showing the connectivity to 10 neighboring Gd atoms from which two are connected directly through the P1 and P3 phosphonate groups and eight across the diamantane moiety of the linker. The doubly bridged Gd chains run parallel to the *b*-direction and are up-and-down connected to four parallel chains. a) View perpendicular to the b-direction, b) view approximately along the b-direction depicting the extended 3D network. The diamantane unit is replaced by a direct P—P connector in magenta for clarity (the crystal water molecules are not shown). Symmetry codes: (i) $-x+1/2$, y − 1/2, $-z+3/2$; (ii) x − 1, y, z; (iii) $-x+1/2$, $y+1/2$, $-z+3/2$; (v) $-x+1$, −y, $-z+1$. See Figure S18 and S25, Supporting Information for the corresponding images of **1-m** and **3**.

In the half-occupied linker, which sits on a special position, each phosphonate bridges between two Ln atoms, and the linker as a whole then connects four Ln atoms. Each Ln atom is in total connected to 10 other Ln atoms, with two through the direct phosphonate P1 and P3 bridging action and eight connected across the diamantane moiety of the linker (**Figure** 7, **8**a).

The direct phosphonate bridging action between two adjacent Ln atoms leads to a corrugated doubly bridged Ln-phosphonate chain (Figure 8a) which is "left-and-right" connected to four adjacent strands giving 3D 10-c uni-nodal networks (Figure 8b) with the point symbol $3^{12}.4^{22}.5^{10}.6$ as analyzed by ToposPro.[45,58]

As seen in **1-o**, and also in **1-m**, **2**, and **3**, the H-atoms of the hydrogenphosphonate groups (-PO_3H^-) are all involved in hydrogen bonding, either to other phosphonate groups or to the crystal water molecules. The hydrogen bonding schemes for **1-m**, **2**, and **3** are shown in Figures S20, S23, and S27, Supporting Information, respectively; a small graph set analysis is given in Section S11, Supporting Information, with Figure S28, Supporting Information.

At last, the hydrophobic interactions between the diamantane moieties within the hydrophobic layers deserve a mention. The weak C—H—H—C contacts could play a role in stabilizing hydrophobic structures, when present in large numbers (the "sticky finger interactions"). In the presented structures their role is secondary, and the contact length tends to be quite long, suggesting mere dispersion/vdW interactions. This is expected, because the primary structure-defining forces are the metal-phosphonate coordination and H—bonding, and the residual-space filling water molecules with other constituents of the polar layers play a role in defining the overall density of the structure rather than the interaction between the diamantane moieties.

3. Conclusions

The structural investigations of the presented lanthanide hydrogenphosphonate frameworks reveal distinct coordination environments depending on the ionic radii of the respective metal centers and the dimensionality of the network. In the 2D network, the largest Ln^{3+} ion in the series here, Eu^{3+} adopts the expected eightfold coordination. In the isostructural 3D networks, Eu^{3+}, Gd^{3+}, and Er^{3+} all tend to a more unusual sixfold coordination in a distorted octahedron. While Eu^{3+} and Gd^{3+} in these 3D networks still have a long Ln—O bond, Er^{3+} has an unequivocal coordination number (CN) of six. This finding emphasizes the critical role of constraints of a coordination network which apparently overrules typical CN preferences of eight to nine of Ln^{3+} ions. Simultaneously, the Ln ions need to be adaptable in their coordination number for the formation of the phosphonate-based frameworks. Further studies will expand the range of Ln ions to verify the above hypothesis about CN and network dimensionality.

4. Experimental Section

Chemicals: All chemicals were used as received from suppliers in reagent grade quality (full list in Table S1, Supporting Information).

Single-Crystal X-Ray Crystallography: Data collection was carried out on a Rigaku XtaLAB Synergy (Rigaku, Tokyo, Japan), Dualflex, HyPix diffractometer with a micro-focus X-ray tube with Cu-Kα radiation (λ = 1.54182 Å). A polarized-light Leica M80 microscope (Leica, Wetzlar, Germany) was used to choose suitable single crystals which were covered with oil on a cryo-loop. Temperature for data collection was 150 K. CRYSALISPRO was used for cell refinement, data reduction, and absorption correction.[59] The crystal structures were solved using OLEX2−1.5 with SHELXT and refined with SHELXL.[60–62] All nonhydrogen atoms were refined with anisotropic displacement parameters. All hydrogen atoms on C were positioned geometrically. Hydrogen atoms on O were found and refined with Uiso(H) = 1.5 Ueq(O). Crystal and structure refinement data of diamantane-4,9-bis (methyl hydrogenphosphonate) (Diam($PO_3HMe)_2$) and diamantane-4-chloro-9-(methyl hydrogenphosphonate) (DiamCl(PO_3HMe) are summarized in **Table 1**, for the lanthanide diamantane-phosphonate networks in **Table 2**. The crystallographic data (excluding structure factors) for the structures were deposited with the Cambridge Crystallographic Data Centre (CCDC deposition numbers 2,455,260–2,455,265) and can be obtained free of charge via www.ccdc.cam.ac.uk/data_request/cif.[63]

Powder X-Ray Diffraction (PXRD): PXRD patterns were measured over the 2θ range of 5–50° in reflective mode using a Rigaku MiniFlex600 or a Bruker D2 Phaser diffractometer with graphite monochromated Cu-Kα irradiation (λ = 1.54182 Å) at room temperature. The Rigaku MiniFlex600 was operated using a 600 W source (40 kV, 15 mA) and equipped with a HyPix-400 MF 2D hybrid pixel array detector (HPAD); the measurements were performed with a 0.01° step size. The Bruker D2 Phaser diffractometer was operated with a 300 W source (30 kV, 10 mA) and equipped with a Lynxeye detector.

Thermogravimetric Analysis (TGA): Thermogravimetric analyses were performed using a Netzsch TG209 F3 Tarsus under synthetic air with a heating ramp of 10 K min^{-1} up to 1000 °C.

NMR Spectra: NMR-spectra were measured with a Bruker Avance NEO evo—600 (^{1}H: 600 MHz, ^{31}P: 242.9 MHz). ^{1}H-NMR chemical shifts are referenced to the residual solvent signal versus TMS ($\delta CHCl_3$ = 7.26 ppm). $^{31}P\{^1H\}$-NMR chemical shifts are externally referenced to H_3PO_4.

Synthesis of Diamantane-4,9-Bis(Dichlorophosphoryl), Diam($POCl_2)_2$: Procedure a: Diamantane-4,9-bis(dichlorophosphoryl) was synthesized according to a modified version of a method developed by Fokin et al. (Scheme 1).[41] The amount of 597 mg (2.7 mmol) of 4,9-dihydroxydiamantane was added to a 100 mL two-necked round bottom flask, followed by the addition of 15 mL of trifluoroacetic acid and 1.5 mL (17.1 mmol) of PCl_3. The reaction mixture was refluxed for 3.5 h and subsequently quenched with water. A solid product was isolated by filtration and dried in a vacuum oven at 60 °C overnight. While the literature reports a yield of ≈90%, consistent reproducibility proved challenging across multiple batches. Notably, product precipitation occurred inconsistently, with some reactions yielding immediate precipitates within 30 min, while others remained in solution until quenching with cold water. The ^{1}H and ^{31}P NMR analysis (see Figures S7 and S8, Supporting Information) revealed the presence of at least DiamCl($POCl_2$) and Diam($POCl_2)_2$ (cf. Scheme 1) in a ratio of ≈2.6:1 which could not be separated by column chromatography in our hands.

Procedure b: To explore alternative reaction conditions, a solvothermal approach was investigated. For this, 55 mg (0.25 mmol) of 4,9-dihydroxydiamantane, 3 mL of trifluoroacetic acid, and 0.2 mL (2.3 mmol) of PCl_3 were combined in a 10 mL Teflon-lined steel autoclave. The reaction mixture was heated to 95 °C within 1.5 h, maintained at this temperature for 6 h, and then gradually cooled to room temperature. A solid product was isolated in about 10% yield

Table 1. Crystal and structure refinement data for $Diam(PO_3HMe)_2$ and $DiamCl(PO_3HMe)$.

	$Diam(PO_3HMe)_2$	$DiamCl(PO_3HMe)$
Empirical formula	$C_{16}H_{26}O_6P_2{\cdot}3(H_2O)$	$C_{15}H_{22}ClO_3P{\cdot}H_2O$
M/g mol^{-1}	430.35	334.76
T/K	150	150
Wavelength/Å[a]	1.54184	1.54184
Crystal system	Monoclinic	Monoclinic
Space group	*C*2/*c*	$P2_1/c$
a/Å	6.84902(12)	16.7708(2)
b/Å	11.2619(2)	7.3404(1)
c/Å	25.2013(5)	12.6215(2)
β/deg	95.9935(16)	92.134(1)
V/Å^3	1933.22(6)	1552.68(4)
Z	4	4
Calcd. Density/g cm^{-3}	1.479	1.432
μ/mm^{-1}	2.47	3.27
F(000)/e	920	712
Crystal size/mm^3	0.65 × 0.31 × 0.18	0.15 × 0.08 × 0.05
θ Range/deg	3.5–78.4	2.6–79.7
Reflections collected	25,193	29,195
Independent reflections; R_{int}	1966; 0.079	3274; 0.036
Completeness to θ_{max}/%	1.000	1.000
R1; wR2 ($I > 2\,\sigma(I)$)[a]	0.1016; 0.2726	0.0448; 0.1198
R1; wR2 (all data)[b]	0.1010; 0.2736	0.0406; 0.1167
Goodness-of-fit[c]	1.14	1.12
$\Delta\rho$fin (max; min)/e Å^{-3}[d]	1.12; −0.72	0.45; −0.45
CCDC no.	2,455,260	2,455,261

[a]$R1 = \Sigma||F_o| - |F_c||/\Sigma|F_o|$; [b]$wR2\ [\Sigma w(F_o^2 - F_c^2)^2/\Sigma[w(F_o^2)^2]^{1/2}$, $w = [\sigma^2(F_o^2) + (aP)^2 + bP]^{-1}$, where $P = (F_o^2 + 2F_c^2)/3$, *a* and *b* are constants adjusted by the program; [c]$GoF = S = [\Sigma w(F_o^2 - F_c^2)^2/(n_{obs} - n_{param})]^{1/2}$, where n_{obs} is the number of data and n_{param} the number of refined parameters; [d]Largest peak and hole in final difference map.

Table 2. Crystal and structure refinement data for **1-o**, **1-m**, **2**, and **3**.

	$\{[EuL_{1.5}(H_2O)_4]{\cdot}H_2O\}_n$, (1-o)	$\{[EuL_{1.5}(H_2O)]{\cdot}H_2O\}_n$, (1-m)	$\{[GdL_{1.5}(H_2O)]{\cdot}H_2O\}_n$, (2)	$\{[ErL_{1.5}(H_2O)]{\cdot}H_2O\}_n$, (3)
Empirical formula	$C_{21}H_{38}EuO_{13}P_3{\cdot}H_2O$	$C_{21}H_{32}EuO_{10}P_3{\cdot}H_2O$	$C_{21}H_{32}GdO_{10}P_3{\cdot}H_2O$	$C_{21}H_{32}ErO_{10}P_3{\cdot}H_2O$
M/g mol^{-1}	761.40	707.35	712.64	722.65
T/K	150	150	150	150
Wavelength/Å[a]	1.54184	1.54184	1.54184	1.54184
Crystal system	Orthorhombic	Monoclinic	Monoclinic	Monoclinic
Space group	*Pbca*	$P2_1/n$	$P2_1/n$	$P2_1/n$
a/Å	11.4048(2)	11.8043(2)	11.9044(2)	11.9973(1)
b/Å	19.9120(2)	11.1236(2)	11.0888(2)	10.9778(1)
c/Å	23.4321(3)	19.8966(4)	19.9039(3)	19.7560(1)
β/deg	90	104.673(2)	103.737(2)	102.836(1)
V/Å^3	5321.25(13)	2527.35(8)	2552.27(8)	2536.92(4)
Z	8	4	4	4
Calcd. density/g cm^{-3}	1.901	1.859	1.855	1.892
μ/mm^{-1}	19.22	20.22	19.10	8.45
F(000)/e	3088	1424	1428	1444
Crystal size/mm^3	0.22 × 0.12 × 0.06	0.25 × 0.2 × 0.05	0.15 × 0.12 × 0.08	0.44 × 0.08 × 0.04
θ Range/deg	3.8–77.4	4.0–79.5	4.0–77.1	4.0–78.1
Reflections collected	33,907	25,766	78,115	81,749
Independent reflections; R_{int}	5374; 0.052	5331; 0.052	5314; 0.078	5187; 0.062
Completeness to θ_{max}/%	0.999	0.9998	1.000	1.000
R1; wR2 ($I > 2\,\sigma(I)$)[a]	0.0359; 0.0973	0.0498; 0.1415	0.0490; 0.1383	0.0357; 0.993
R1; wR2 (all data)[b]	0.0339; 0.0957	0.0527; 0.1447	0.0459; 0.1350	0.0343; 0.0978
Goodness-of-fit[c]	1.045	1.13	1.143	1.087
$\Delta\rho$fin (max; min)/e Å−3[d]	1.04; −1.26	1.73; −1.29	0.978; −2.01	1.49; −1.39
CCDC no.	2,455,262	2,455,263	2,455,264	2,455,265

[a]$R1 = \Sigma||F_o| - |F_c||/\Sigma|F_o|$; [b]$wR2\ [\Sigma w(F_o^2 - F_c^2)^2/\Sigma[w(F_o^2)^2]^{1/2}$, $w = [\sigma^2(F_o^2) + (aP)^2 + bP]^{-1}$, where $P = (F_o^2 + 2F_c^2)/3$, *a* and *b* are constants adjusted by the program; [c]$GoF = S = [\Sigma w(F_o^2 - F_c^2)^2/(n_{obs} - n_{param})]^{1/2}$, where n_{obs} is the number of data and n_{param} the number of refined parameters; [d]Largest peak and hole in final difference map.

by filtration, washed with cold ultrapure water, and dried in a vacuum oven at 60 °C for 1 day. The ^{1}H and ^{31}P NMR analysis (see Figures S9 and S10, Supporting Information) revealed again the presence of DiamCl($POCl_2$) and Diam($POCl_2$)$_2$ (cf. Scheme 1) in a ratio of about 0.8:1. Elevating the temperature or extending the reaction time did not significantly improve the yield or selectivity of the reaction towards Diam($POCl_2$)$_2$.

Synthesis of Diamantane-4,9-Bis(Methyl Hydrogenphosphonate, Diam(PO_3HMe)$_2$, and Diamantane-4-Chloro-9-(Methyl Hydrogenphosphonate) (DiamCl(PO_3HMe)) Monohydrate: The amount of 5.4 mg (0.01 mmol) of the above mixture from procedure b which contained diamantane-4,-9bis(dichlorophosphoryl) and diamantane-4-chloro-9-(dichloro-phosphoryl)) together with 5.8 mg (0.02 mmol) of $Mg(NO_3)_2{\cdot}6H_2O$ was placed in a Pyrex glass tube. Subsequently, 2 mL of methanol, 100 µL of ultrapure water, and 250 µL of glacial acetic acid were added sequentially. The Pyrex tube was sealed and subjected to ultrasonic homogenization for 10 min. The tube was then transferred to a synthesis oven and heated at 80 °C for 72 h. From the product mixture crystals of Diam(PO_3HMe)$_2$, diamantane-4-chloro-9-(methyl hydrogenphosphonate) (DiamCl(PO_3HMe)) and of unreacted Diam($POCl_2$)$_2$ were obtained as thin, colorless rods and thin plates and only identified from single-crystal X-ray analysis (no further analyses were performed).

Synthesis of {[EuL$_{1.5}$(H_2O)$_4$]·H_2O}$_n$, 1-o: In a typical procedure, 18.7 mg (0.044 mmol) of $Eu(NO_3)_3{\cdot}5H_2O$, 5.5 mg (0.013 mmol) of commercial diamantane-4,9-bis(dichlorophosphoryl), 3.1 mg (0.02 mmol) of 4,4′-bipyridine, and 11.2 mg (0.10 mmol) of p-ethylphosphonic acid (EtPA) were combined in a 10 mL Teflon liner. Ultrapure water (5 mL) was added, and the mixture was stirred for ≈3 min with a small stirring bar on a stirring plate. The Teflon liner was then sealed in a stainless-steel autoclave and heated to 190 °C within 8 h. The reaction was maintained at 190 °C for 5 days before being gradually cooled to room temperature over 16 h. The resulting product was transferred to a centrifuge tube and washed several times with ultrapure water. The product consisted of a mixture of white microcrystalline powder and thin, colorless needles. As it was not possible to further purify the compound (see Figure S1A, Supporting Information), no further analyses such as PXRD or TGA could be performed.

Synthesis of {[Eu(L)$_{1.5}$(H_2O)]·H_2O}$_n$, 1-m: The hydrothermal synthesis was carried out as for **1-o**, combining $Eu(NO_3)_3{\cdot}5H_2O$ (124.1 mg, 0.29 mmol), 42.2 mg (0.10 mmol) of commercial diamantane-4,9-bis (dichlorophosphoryl), 23.4 mg (0.15 mmol) of 4,4′-bipyridine, 37.4 mg (0.34 mmol) p-ethylphosphonic acid, and 10 mL of water. The resulting product was thoroughly washed with ultrapure water and methanol and obtained as colorless needles/rods (see Figure S1B, Supporting Information). The product was dried overnight in a vacuum oven at 60 °C for further analysis. The powder X-ray diffractogram and thermogravimetric analysis are given in Figures S2 and S4, Supporting Information, respectively. Compound **1-m** could also be obtained without 4,4′-bpy.

Yield: 35.4 mg, 75% based on linker.

Synthesis of {[Gd(L)$_{1.5}$(H_2O)]·H_2O}$_n$, 2: The hydrothermal synthesis was carried out as for **1-o**, from 130.9 mg (0.29 mmol) of $Gd(NO_3)_3{\cdot}5H_2O$, 42.1 mg (0.10 mmol) of commercial diamantane-4,9-bis(dichlorophosphoryl), 23.4 mg (0.15 mmol) of 4,4′-bipyridine, 37.4 mg (0.34 mmol) p-ethylphosphonic acid, and 10 mL of water with heating to 180 °C. Washing and drying were carried out analogously to **1-m**. The resulting product was isolated as thin, colorless needles (see Figure S1C, Supporting Information). To further characterize compound **2**, PXRD and TGA are shown in Figure S3 and S5, Supporting Information, respectively.

Yield: 42.8 mg, 88% based on linker.

Synthesis of {[Er(L)$_{1.5}$(H_2O)]·H_2O}$_n$, 3: The hydrothermal synthesis was carried out as for **1-o**, from 128.6 mg (0.29 mmol) of $Er(NO_3)_3{\cdot}5H_2O$, 42.0 mg (0.10 mmol) of diamantane-4,9-bis(dichlorophosphoryl), and 15.7 mg (0.14 mmol) of 1,4-diazabicyclo[2.2.2]octane, 37.3 mg (0.34 mmol) p-ethylphosphonic acid, and 5 mL of water. Washing and drying were carried out analogously to **1-m**. The resulting product was isolated as thin, colorless needles (see Figure S1D, Supporting Information), with some powdery by-product which could not be removed by washing. PXRD and TGA are displayed in Figure S3 and S6, Supporting Information, respectively.

Yield: 50.6 mg, 76% based on linker.

Acknowledgements

The Rigaku X-ray diffractometer was funded by the Deutsche Forschungsgemeinschaft, DFG through grant 440366605. The Open Access funding was enabled and organized by Projekt DEAL. The authors thank Dr. István Boldog for initiation of the work on diamantane coordination polymers by formulating the general goal and for synthetic advices during the initial stages of the project. We thank Prof. Dr. Peter Schreiner at Univ. Gießen and Dr. Boryslav O. Tkachenko from TransMIT for providing the samples of the ligands and supporting our work on adamantane derivatives with their valuable expertise.

Open Access funding enabled and organized by Projekt DEAL.

Conflict of Interest

The authors declare no conflict of interest.

Data Availability Statement

The data that support the findings of this study are available in the supplementary material of this article.

Keywords: coordination networks · diamandoids · lanthanide · organophosphonates · phosphonic acid esters

[1] D. Sahoo, R. Suriyanarayanan, V. Chandrasekhar, *Dalton Trans.* **2014**, *43*, 10989.
[2] K. Maeda, *Microporous Mesoporous Mater.* **2004**, *73*, 47.
[3] T. Rhauderwiek, K. Wolkersdörfer, S. Øien-Ødegaard, K.-P. Lillerud, M. Wark, N. Stock, *Chem. Commun.* **2018**, *54*, 389.
[4] T. Rhauderwiek, H. Zhao, P. Hirschle, M. Döblinger, B. Bueken, H. Reinsch, D. De Vos, S. Wuttke, U. Kolb, N. Stock, *Chem. Sci.* **2018**, *9*, 5467.
[5] M. J. Białek, J. K. Zaręba, J. Janczak, J. Zoń, *Cryst. Growth Des.* **2013**, *13*, 4039.
[6] G. Yücesan, Y. Zorlu, M. Stricker, J. Beckmann, *Coord. Chem. Rev.* **2018**, *369*, 105.
[7] T. Zheng, W. Tan, L.-M. Zheng, *Acc. Chem. Res.* **2024**, *57*, 2973.
[8] C. Livingston, G. J. Blanchard, *Langmuir* **2021**, *37*, 4658.
[9] R. G. Franz, *AAPS PharmSci.* **2001**, *3*, 10.
[10] S. S. Iremonger, J. Liang, R. Vaidhyanathan, I. Martens, G. K. H. Shimizu, T. D. Daff, M. Z. Aghaji, S. Yeganegi, T. K. Woo, *J. Am. Chem. Soc.* **2011**, *133*, 20048.

[11] A. B. Lysenko, G. A. Senchyk, J. Lincke, D. Lässig, A. A. Fokin, E. D. Butova, P. R. Schreiner, H. Krautscheid, K. V. Domasevitch, *Dalton Trans.* **2010**, *39*, 4223.
[12] V. Gvilava, M. Vieten, R. Oestreich, D. Woschko, M. Steinert, I. Boldog, R. Bulánek, N. A. Fokina, P. R. Schreiner, C. Janiak, *CrystEngComm* **2022**, *24*, 7530.
[13] V. V. Danilenko, *Solid State Phys.* **2004**, *46*, 595.
[14] J. Goura, V. Chandrasekhar, *Chem. Rev.* **2015**, *115*, 6854.
[15] I. Koehne, A. Lik, M. Gerstel, C. Bruhn, J. P. Reithmaier, M. Benyoucef, R. Pietschnig, *Dalton Trans.* **2020**, *49*, 16683.
[16] W. A. Clay, J. E. P. Dahl, R. M. K. Carlson, N. A. Melosh, Z.-X. Shen, *Rep. Prog. Phys.* **2015**, *78*, 016501.
[17] M. A. Gunawan, J.-C. Hierso, D. Poinsot, A. A. Fokin, N. A. Fokina, B. A. Tkachenko, P. R. Schreiner, *New J. Chem.* **2014**, *38*, 28.
[18] Y. Zhou, A. D. Brittain, D. Kong, M. Xiao, Y. Meng, L. Sun, *J. Mater. Chem. C* **2015**, *3*, 6947.
[19] W. L. Yang, J. D. Fabbri, T. M. Willey, J. R. I. Lee, J. E. Dahl, R. M. K. Carlson, P. R. Schreiner, A. A. Fokin, B. A. Tkachenko, N. A. Fokina, W. Meevasana, N. Mannella, K. Tanaka, X. J. Zhou, T. van Buuren, M. A. Kelly, Z. Hussain, N. A. Melosh, Z.-X. Shen, *Science* **2007**, *316*, 1460.
[20] V. V. Bakhonsky, A. A. Pashenko, J. Becker, H. Hausmann, H. J. M. De Groot, H. S. Overkleeft, A. A. Fokin, P. R. Schreiner, *Dalton Trans.* **2020**, *49*, 14009.
[21] K. Chainok, N. Ponjan, C. Theppitak, P. Khemthong, F. Kielar, W. Dungkaew, Y. Zhou, S. R. Batten, *CrystEngComm* **2018**, *20*, 7446.
[22] S. Jiajaroen, W. Dungkaew, F. Kielar, M. Sukwattanasinitt, S. Sahasithiwat, H. Zenno, S. Hayami, M. Azam, S. I. Al-Resayes, K. Chainok, *Dalton Trans.* **2022**, *51*, 7420.
[23] M. Armaghan, K. Darzinezhad, M. M. Amini, C. Janiak, *Z. Naturforsch.* **2021**, *76*, 699.
[24] D.-H. Chen, A. E. Sedykh, G. E. Gomez, B. L. Neumeier, J. C. C. Santos, V. Gvilava, R. Maile, C. Feldmann, C. Wöll, C. Janiak, K. Müller-Buschbaum, E. Redel, *Adv. Mater. Interfaces* **2020**, *7*, 2000929.
[25] J. Dechnik, F. Mühlbach, D. Dietrich, T. Wehner, M. Gutmann, T. Lühmann, L. Meinel, C. Janiak, K. Müller-Buschbaum, *Eur. J. Inorg. Chem.* **2016**, 4408.
[26] X. Guo, G. Zhu, Z. Li, F. Sun, Z. Yang, S. Qiu, *Chem. Commun.* **2006**, 3172.
[27] M. Raizada, F. Sama, M. Ashafaq, M. Shahid, M. Khalid, M. Ahmad, Z. A. Siddiqi, *Polyhedron* **2018**, *139*, 131.
[28] B. Gil-Hernández, J. K. Maclaren, H. A. Höppe, J. Pasan, J. Sanchiz, C. Janiak, *CrystEngComm* **2012**, *14*, 2635.
[29] J. R. Choi, T. Tachikawa, M. Fujitsuka, T. Majima, *Langmuir* **2010**, *26*, 10437.
[30] J. Lee, O. K. Farha, J. Roberts, K. A. Scheidt, S. T. Nguyen, J. T. Hupp, *Chem. Soc. Rev.* **2009**, *38*, 1450.
[31] D. Bejan, L. G. Bahrin, S. Shova, N. L. Marangoci, Ü. Kökçam-Demir, V. Lozan, C. Janiak, *Molecules* **2020**, *25*, 3055.
[32] M. Boone, F. Artizzu, J. Goura, D. Mara, R. V. Deun, M. D'hooghe, *Coord. Chem. Rev.* **2024**, *501*, 215525.
[33] L. V. Meyer, F. Schönfeld, K. Müller-Buschbaum, *Chem. Commun.* **2014**, *50*, 8093.
[34] L. V. Meyer, F. Schönfeld, A. Zurawski, M. Mai, C. Feldmann, K. Müller-Buschbaum, *Dalton Trans.* **2015**, *44*, 4070.
[35] M. Bazaga-García, I. R. Salcedo, R. M. P. Colodrero, K. Xanthopoulos, D. Villemin, N. Stock, M. López-González, C. del Río, E. R. Losilla, A. Cabeza, K. D. Demadis, P. Olivera-Pastor, *Chem. Mater.* **2019**, *31*, 9625.
[36] A. Dutta, Y. Pan, J.-Q. Liu, A. Kumar, *Coord. Chem. Rev.* **2021**, *445*, 214074.
[37] W. Fan, X. Zhang, Z. Kang, X. Liu, D. Sun, *Coord. Chem. Rev.* **2021**, *443*, 213968.
[38] S. Ondrušová, M. Kloda, J. Rohlíček, M. Taddei, J. K. Zaręba, J. Demel, *Inorg. Chem.* **2022**, *61*, 18990.
[39] T. Devic, C. Serra, *Chem. Soc. Rev.* **2014**, *43*, 6097.
[40] S. J. I. Shearan, N. Stock, F. Emmerling, J. Demel, P. A. Wright, K. D. Demadis, M. Vassakai, F. Costantino, R. Vivani, S. Sallard, I. R. Salcedo, A. Cabeza, M. Taddei, *Crystals* **2019**, *9*, 270.
[41] A. A. Fokin, R. I. Yurchenko, B. A. Tkachenko, N. A. Fokina, M. A. Gunawan, D. Poinsot, J. E. P. Dahl, R. M. K. Carlson, M. Serafin, H. Cattey, J.-C. Hierso, P. R. Schreiner, *J. Org. Chem.* **2014**, *79*, 5369.
[42] F. Bigdeli, M. N. A. Fetzer, B. Nis, A. Morsali, C. Janiak, *J. Mater. Chem. A* **2023**, *11*, 22105.
[43] J. Łuczak, M. Kroczewska, M. Baluk, J. Sowik, P. Mazierski, A. Zaleska-Medynska, *Adv. Colloid Interface Sci.* **2023**, *314*, 102864.
[44] F. Gándara, V. A. de la Peña-O'Shea, F. Illas, N. Snejko, D. M. Proserpio, E. Gutiérrez-Puebla, M. A. Monge, *Inorg. Chem.* **2009**, *48*, 4707.
[45] M. Llunell, D. Casanova, J. Cirera, P. Alemany, S. Alvarez, in *SHAPE, version 2.1*, Universitat de Barcelona, Barcelona, Spain **2013**.
[46] ToposPro Version 5531 (64 bit), https://topospro.com/.
[47] M. Seitz, A. G. Oliver, K. N. Raymond, *J. Am. Chem. Soc.* **2007**, *129*, 11153.
[48] G. Ferru, B. Reinhart, M. K. Bera, M. O. de la Cruz, B. Qiao, R. J. Ellis, *Chem. Eur. J.* **2016**, *22*, 6899.
[49] F. G. Chávez, H. I. Beltrán, *New J. Chem.* **2021**, *45*, 6600.
[50] J.-C. G. Bünzli, *J. Coord. Chem.* **2014**, *67*, 3706.
[51] S. A. Cotton, P. R. Raithby, *Coord. Chem. Rev.* **2017**, *340*, 220.
[52] T.-T. Wang, Y.-M. Su, C.-Q. Jiao, X.-O. Cai, H.-M. Sun, Y.-Y. Zhu, Z.-G. Sun, *New J. Chem.* **2018**, *42*, 1235.
[53] E. C. Lewandowski, C. B. Arban, M. P. Deal, A. L. Batchev, M. J. Allen, *Chem. Commun.* **2024**, *60*, 10655.
[54] F. Marchetti, C. Pettinari, R. Pettinari, *Coord. Chem. Rev.* **2005**, *249*, 2909.
[55] K. Dehnicke, A. Greiner, *Angew. Chem. Int. Ed.* **2003**, *42*, 1340.
[56] B. Na, X.-J. Zhang, W. Shi, Y.-Q. Zhang, B.-W. Wang, C. Gao, S. Gao, P. Cheng, *Chem. Eur. J.* **2014**, *20*, 15975.
[57] A. A. Trifonov, D. M. Lyubov, *Coord. Chem. Rev.* **2017**, *340*, 10.
[58] V. A. Blatov, A. P. Shevchenko, D. M. Proserpio, *Cryst. Growth Des.* **2014**, *14*, 3576.
[59] CrysAlisPro, *Rigaku Oxford Diffraction; Release 1.171.40.103a; Agilent*; Agilent Technologies Ltd.: Yarnton, UK **2014**, https://rigaku.com/products/crystallography/x-ray-diffraction/application-notes/px018-crysalispro-software-package-single-crystal.
[60] O. V. Dolomanov, L. J. Bourhis, R. J. Gildea, J. A. K. Howard, H. Puschmann, *J. Appl. Crystallogr.* **2009**, *42*, 339.
[61] G. M. Sheldrick, *Acta Crystallogr. Sect. A Found. Adv.* **2015**, *71*, 3.
[62] G. M. Sheldrick, *Acta Crystallogr. Sect. C Struct. Chem.* **2015**, *71*, 3.
[63] Deposition numbers 2455260 (for Diam(PO3HMe)2), 2455261 (for DiamCl(PO3HMe)), 2455262 (for **1-o**), 2455263 (for **1-m**), 2455264 (for **2**), and 2455261 (for **3**) contain the supplementary crystallographic data for this paper. These data are provided free of charge by the joint Cambridge Crystallographic Data Centre and Fachinformationszentrum Karlsruhe Access Structures service, www.ccdc.cam.ac.uk/data_request/cif.

Manuscript received: August 1, 2025
Revised manuscript received: September 29, 2025
Version of record online: October 22, 2025

